Structural characterization and transdermal delivery studies on sugar microneedles: Experimental and finite element modelling analyses

Eriketi Z. Loizidou[a,b], Nicholas A. Williams[a], David A. Barrow*[b], Mark J. Eaton[b], John McCrory[b], Sam L. Evans[b], Chris J. Allender**[a]

[a]Cardiff University, School of Pharmacy, CF10 3NB, United Kingdom

[b]Cardiff University, School of Engineering, CF24 3AA, United Kingdom

* Corresponding author. Address: Cardiff School of Engineering, Cardiff University, 1-5 The Parade, Cardiff CF24 3AA, Cardiff, UK; Tel. +44(0)2920875921; Email address: barrow@cardiff.ac.uk

** Corresponding author. Address: School of Pharmacy, Cardiff University, Redwood Building, King Edward VII Ave, Cardiff CF10 3NB, Cardiff, UK; Tel. +44(0)2920875824; Email address: allendercj@cf.ac.uk

Abstract

Dissolving microneedles are especially attractive for transdermal drug delivery as they are associated with improved patient compliance and safety. Furthermore, microneedles made of sugars offer the added benefit of biomolecule stabilisation making them ideal candidates for delivering biological agents such as proteins, peptides and nucleic acids. In this study, we performed experimental and finite element analyses to study the mechanical properties of sugar microneedles and evaluate the effect of sugar composition on microneedle ability to penetrate and deliver drug to the skin. Results showed that microneedles made of carboxymethylcellulose / maltose are superior to those made of carboxymethylcellulose / trehalose and carboxymethylcellulose / sucrose in terms of mechanical strength and the ability to deliver drug. Buckling was predicted to be the main mode of microneedle failure and the order of buckling was positively correlated to the Young's modulus values of the sugar constituents of each microneedle.

Keywords

Sugar microneedles, skin penetration, confocal microscopy, structural mechanics simulations, Young's modulus, buckling, von Mises stress, drug delivery

1. Introduction

Microneedles offer a promising approach for delivering therapeutic compounds through the skin, thus avoiding the gastrointestinal and hepatic first-pass metabolism that can degrade the bioactive compounds, as well as the discomfort and pain associated with hypodermic delivery [1]. Furthermore, readily dissolving microneedles offer the added benefit of being able to either deliver secondary controlled delivery vectors or a simple bolus dose.

Sugars are particularly attractive materials for delivering biomolecules via microneedles because in addition to, in the right combinations, forming mechanically strong microneedles that can penetrate the skin and rapidly dissolve, they are also known to act as stabilising agents. Sugars have commonly been used to increase the stability of nucleic acids and proteins, specifically saccharide excipients have been used to stabilise plasmid DNA [2] and human erythropoietin alfa [3] coated on the surface of microneedles. Additionally, sugars have been used in vaccine coating formulations for microneedle-mediated delivery [4–11]. Solid microneedle arrays made entirely out of sugars and encapsulating live recombinant human adenovirus type 5 have been shown to retain bioactivity, inducing potent multifunctional CD8+ T-cell responses, when administered through the skin of mice, at levels equivalent with conventional injectable routes [12]. In another example, human growth hormone (hGH) encapsulated within dissolving microneedle patches made of carboxymethylcellulose and trehalose demonstrated similar pharmacokinetics to conventional subcutaneous injections and retained activity for up to 15 months of storage at room temperature and humidity [13].

The forces that microneedles experience, when penetrating the skin, are typically dependent on microneedle material and geometry. The effect of microneedle geometry such as needle length, and shape (conical and pyramidal triangular and square) has been examined through experiments and computational modeling [14–17]. Studies using the numerical simulator ANSYS showed that circular microneedles experience less bending stress than rectangular and square pyramidal microneedles [14]. In a separate study square pyramidal microneedles demonstrated enhanced skin penetration compared to conical microneedles whilst simulation analysis also predicted a lower force of failure. The effect of material was also examined using the carbohydrates carboxymethylcellulose and amylopectin as reference materials. Amylopectin, due to its higher Young's modulus value, proved to be a mechanically superior material for microneedles, compared to carboxymethylcellulose [15].

In this study we performed a structural analysis of microneedles made from various sugar materials using both experimental measurements and modelling. Through systematic analysis we examined the effect of sugar composition on the mechanical properties of microneedles and their ability to penetrate and deliver a therapeutic agent to the skin. Microneedle arrays of conical geometry, comprising of 1) carboxymethylcellulose and sucrose (CMC / SUC), 2) carboxymethylcellulose and maltose (CMC / MAL) and 3) carboxymethylcellulose and trehalose dihydrate (CMC / TRD) at a 1:1 combination were prepared using a vacuum deposition method [18] and characterised by brightfield microscopy and SEM. Microneedle skin insertion was tested on porcine skin using brightfield / epi-fluoresence microscopy to

study skin puncture and confocal microscopy to study the skin penetration depth. Tensile tests were used to measure the Young's modulus values of the sugar compositions and finite element analysis, using the Structural Mechanics module of COMSOL Multiphysics, was performed to evaluate the effects of material on the stresses experienced by the microneedles. Using a standard Franz-type diffusion cell setup, the ability of each type of sugar microneedle to deliver propanolol to *ex vivo* porcine skin was also investigated.

2. Material and methods

2.1 Microneedle fabrication

Microneedle arrays consisting of CMC (average MW 250,000, Sigma-Aldrich, UK) and either SUC (Sigma-Aldrich, UK), MAL (20 % solution, Sigma-Aldrich, UK) or TRD (Sigma-Aldrich, UK) were prepared by the vacuum deposition method described by Martin *et al*. [18]. Briefly, 200 μl of 2 % w/v solutions of sugar mixtures (1:1 w/w ratio of i) CMC / SUC, ii) CMC / MAL and iii) CMC / TRD) in water were injected onto a 1 cm^2 inverted cone shaped silicone micromould comprising 324 needles of 750 μm height, 200 μm base diameter, and 600 μm center-to-center spacing under vacuum. Following application of the sugar solutions, vacuum was released and the filled micromoulds were placed in a fume cupboard and allowed to dehydrate at room temperature for 3 days. The resulting microneedle arrays were characterised by brightfield / epi-fluoresence microscopy (Nikon measuring microscope MM-800) and scanning electron microscopy (Carl Zeiss XB1540).

2.2 Tensile tests

Digital Image Correlation (DIC) was used to measure the strain distributions during tensile evaluation. Displacement measurements were made using a Dantec Dynamics DIC system (Dantec Dynamics A/S, Tonsbakken, Denmark) with two cameras and ISTRA4D software, on the narrow part of a “dog bone” structure consisting of the sugar composites used to prepare the microneedles. The strain values used in the analysis were the average strains over the narrow part of the structures, as calculated by the DIC software. “Dog bone” structures were prepared for the three materials (CMC / SUC, CMC / MAL and CMC / TRD) by dissolving the sugar / CMC mixtures in water at 2 % w/v composition, and then layering the solutions on a PDMS sheet, which was left in a fume hood to dehydrate for 3 days. The resulting materials were cut to a “dog bone” shape using a template with a parallel gauge length 40 mm long and 6.5 mm wide. The average thickness of the sugar / CMC layers was 1.2 mm.

2.3 Simulations

Simulations were performed using the Structural Mechanics Module of COMSOL Multiphysics (www.comsol.com). Simulations were performed on a single microneedle, the design of which was based on a 3D cone-shaped structure of dimensions 750 μm height, 200 μm base diameter and 10 μm tip diameter. The needle structures were treated as linear elastic materials using the Young’s modulus values and densities measured for each sugar composition (Table 1), and an estimated value of 0.3 for Poisson’s ratio. Two cylindrical structures were used to simulate the epidermis (including both the stratum corneum and viable epidermis) and dermis of the skin having the

following dimensions, 600 μm diameter and 100 μm height for the epidermis and 600 μm diameter and 1000 μm height for the dermis. The skin structure was treated as a linear elastic material using 1 MPa as the Young's modulus value for the epidermis [19] and 0.066 Mpa for the dermis [20]. Both epidermis and dermis were treated as nearly incompressible materials with Poisson's ratio 0.495. The Solid Mechanics interface was used to define the quantities and features for stress analysis, solving for the displacements. Von Mises stress and microneedle / skin deformation was simulated at static equilibrium using stationary analysis, during axial loading at the base of the needle for force values ranging from 0.1 to 17 N. A fixed constrain was applied at the bottom surface of the dermis and movement of the needle base was allowed only for the axial direction. Linear buckling analysis was used to estimate the critical load at which the microneedle would become unstable. The critical load factor of the microneedles was simulated during axial loading with a 5 N applied force, for the case where one end, the microneedle tip, was fixed in position and the other end, the microneedle base, was allowed to move only in the axial direction.

2.4 Skin preparation

Freshly excised porcine ears, from pigs weighing 70-90 kg, were obtained from a local abattoir (prior to steam cleaning) and washed under cold running water. Full thickness skin was isolated from the underlying cartilage by blunt dissection and any hairs removed using electric clippers. The skin was cut into sections (~ 3 cm^2) and stored at - 20 °C until required.

2.5 Skin penetration

Sections of frozen skin were thawed by briefly soaking in water (37 ^{o}C) and then dried under air. The sugar microneedle arrays (CMC / SUC, CMC / MAL and CMC / TRD) were applied to the skin for 30 seconds with gentle thumb pressure. The punctured skin surface was exposed to green tissue-marking dye (Fisher Scientific, UK) for 15 minutes after which any residual dye was wiped from the skin surface with tissue paper and swabbed clean with tap-water. The treated skin was imaged and recorded under a microscope (Nikon measuring microscope MM-800). Confocal microscopy was used to determine the depth of skin penetration for each sugar microneedle array. Fluorescent sugar microneedles containing AlexaFluor 488 C5 maleimide, 50 μg/ml, (Life Technologies Ltd, UK), were prepared in a procedure similar to the one described in Section 2.1 and skin penetration evaluated using full-thickness cadaver porcine skin previously incubated overnight in phosphate buffered saline (pH 7.4) containing 10 μg/ml Hoechst trihydrochloride trihydrate (Life Technologies Ltd, UK). The fluorescently labelled sugar microneedle arrays were applied to the skin with gentle thumb pressure and after 10 min were removed and the skin samples examined using a Leica SP5 confocal laser-scanning microscope equipped with an Ar laser and 20x objective.

2.6 Drug delivery studies

Sections of frozen porcine skin were thawed in phosphate buffered saline (PBS, composition: NaCl 137 mM, NaH2PO4 10 mM, KCl 2.7 mM, KH2PO4 1.8 mM, pH 7.4) at 37 °C for 30 min and gently dabbed with

absorbent paper towel to remove excess moisture. Sugar microneedles loaded with propanolol hydrochloride (Sigma-Aldrich, UK) at 5 % w/w concentration, were prepared in a procedure similar to the one described in Section 2.1. The propanolol-loaded microneedles were applied to the skin sections with gentle thump pressure for two minutes before loading into custom-built, static Franz-type diffusion cells (average area of tissue exposure 1.32 cm^2) and covered with cling film to prevent evaporative loss. The receptor compartment was filled with 3.5 ml PBS, a micro-magnetic stirrer bar added to provide continuous stirring and the sampling arm capped. The diffusion cells were placed on a submersible magnetic stirring plate in a water bath maintained at 37 °C in order to achieve a skin surface temperature of 32 °C (average skin temperature). At pre-defined time-points (2, 4, 6, 8, 10, 24 and 30 h) 250 μl of the receptor solution was sampled and replaced with 250 μl of 32 °C PBS. After the final time-point (30 h), the donor solution was sampled and the Franz-type cells dismantled. After removing the cling film and remaining microneedle backing, the skin area of drug contact was excised, weighed, homogenised (Precellys®24, Bertin Technologies Inc, Bordeaux, France) and the drug extracted in 4 ml of mobile phase for 36 hours with 10 minutes sonication per sample. Samples were then centrifuged for 5 min (7000 RPM, 2680 g) and the supernatant isolated for analysis.

2.7 Quantification of propanolol

Propanolol hydrochloride was analysed by HPLC. The column was Kromasil C18 column, 5 μm, 250 mm x 4.6 mm i.d column, Supelco Inc) and mobile phase 60 % acetonitrile : 40 % (aq) containing sodium dodecyl sulfate (10 mM), and disodium hydrogen phosphate (10 mM) adjusted to pH 2.3 with

phosphoric acid. Detection was UV (290 nm), injection volume was 20 μl and flow rate 1 ml min^{-1}. The limits of detection and quantification were 0.05 and 0.166 μg ml^{-1} respectively.

3. Results

3.1 Microneedle fabrication and characterisation

Sugar microneedles have been fabricated using different approaches including casting a viscous aqueous solution of sugars onto a microneedle inverse mould and then using centrifugation to force the liquid into the mould [9,15] or by casting sugar-melts in the form of a microneedle array [21]. Microneedles made of maltose have also been prepared by stepwise controlled drawing lithography by controlling the drawing time and the solution viscosity [22].

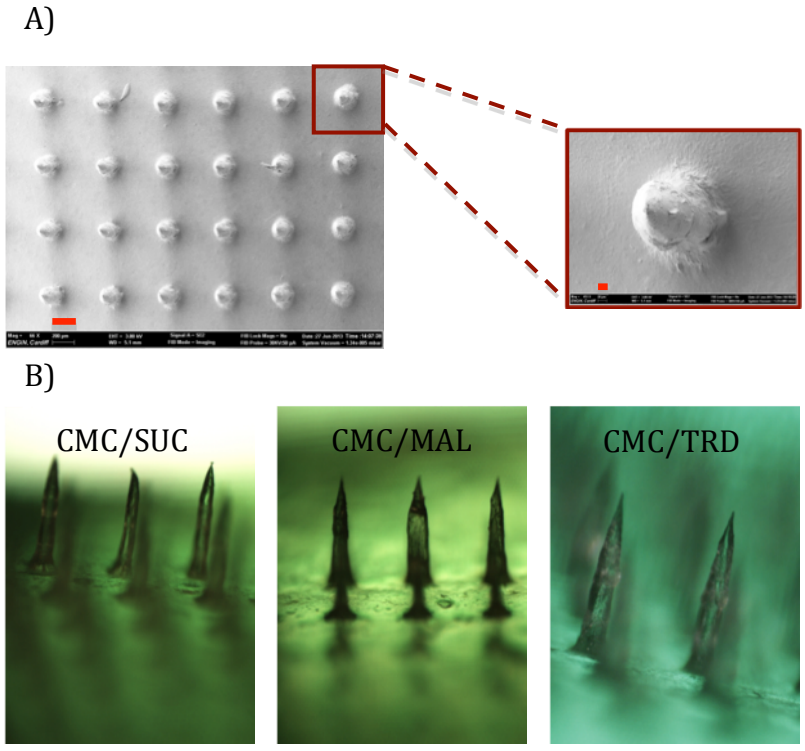

Figure 1: Sugar microneedle array images. A) Scanning electron micrographs of a CMC / TRD microneedle array at low magnification (scale bar = 200μm) and high magnification (scale bar = 20μm). B) Microscopic images (5x objective) of a CMC / SUC, CMC / MAL and CMC / TRD array.

In this study, we used vacuum deposition [18] to prepare the sugar microneedles. The methodology involves depositing a solution onto an inverse microneedle mould, so as to achieve complete coverage, contained within an evacuated chamber. When the vacuum is released gas pressure forces the solution into the mould so as to completely fill the mould's micron-scale cavities. Using this approach microneedle arrays, were prepared using three CMC / sugar composites (CMC / SUC, or CMC / MAL, or CMC / TRD). The resulting microneedle arrays were imaged using SEM and light-microscopy (Fig. 1) and were shown to possess close reciprocal geometries to the mould (750 μm length, 200 μm base diameter, 10 μm tip diameter) and a tip-to-tip needle spacing of 600 μm. The microneedle arrays were stored at ambient temperature and relative humidity and, based on microscopic observation, were capable of retaining an unchanged geometry for at least two months.

3.2 Structural analysis

The mechanical properties of the sugar materials were initially assessed using the load acquired from the test machine and the strain measurements calculated by the DIC analysis. Knowledge of the specimen dimensions allowed the stress to be calculated from the load and so plots of stress against strain were generated (Fig. 2). The CMC / MAL and CMC / TRD sugar combinations showed linear behavior up to the point of failure by fracture. This is typical of brittle materials, such as glass. On the other hand, the CMC / SUC combination was more flexible with some evidence of non-linearity at small strains. However, the linearly elastic region was prominent

and a Young's modulus value was derived. In addition, ultimate tensile strengths were determined at the highest point in the stress / strain curves. The values (Table 1) were subsequently used in microneedle structural mechanics simulations.

Table 1. Young's modulus and ultimate tensile strength for CMC / SUC, CMC / MAL, and CMC / TRD sugar compositions.

Sugar composition	Density	Young's modulus	Ultimate tensile strength
CMC/SUC	1624 Kg/m^2	2.20e7 Pa	2.21e7 Pa
CMC/MAL	1812 Kg/m^2	7.42e9 Pa	7.44e9 Pa
CMC/TRD	1439 Kg/m^2	5.69e9 Pa	5.66e9 Pa

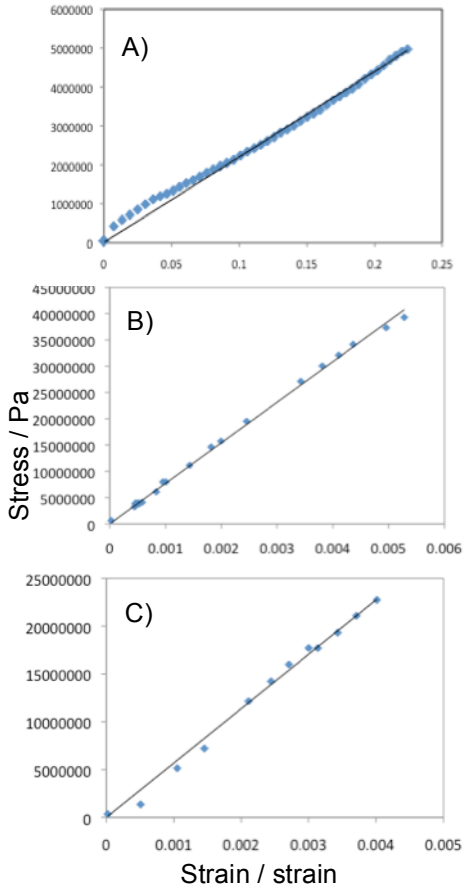

Figure 2: Stress vs. strain curves obtained from tensile tests for sugar materials consisting of A) CMC / SUC, B) CMC / MAL and C) CMC / TRD.

Computationally, the compressive forces acting on the microneedle can be described by the calculated von Mises stress, which refers to the combined principal stresses (in the x, y, z dimensions) acting on an elastic body that is subject to a system of loads. The von Mises values can be used to predict whether a particular design will fail; this will occur if the maximum value of the von Mises stress induced in the material is more than the fracture strength of the material. Furthermore, slender structures often show sudden failure when subject to compressive loads even though the stress at the point of failure is less than the maximum stress that the material can withstand. This mode of failure is known as buckling and can be studied computationally using a linear buckling analysis to estimate the critical load factors. In our simulation analysis we considered an ideal situation where a coaxial force is applied at the base of the microneedle giving rise to compressive and buckling forces only, treating bending forces as negligible. Stationary and linear buckling analyses were employed to solve for the von Mises stresses and the critical buckling loads in a single microneedle with conical geometry and dimensions matching the tested microneedles. Although the skin is not linearly elastic [23] and its deformation may not have been accurately predicted, the microneedle material did exhibit linear behaviour and therefore, a linear elastic model was deemed appropriate to predict the load/stress for the needles. Figure 3A shows a 3D plot of the surface von Mises stress calculated when an axial load is applied to the base of the microneedle. The areas coloured in red depict the areas that experience the most stress.

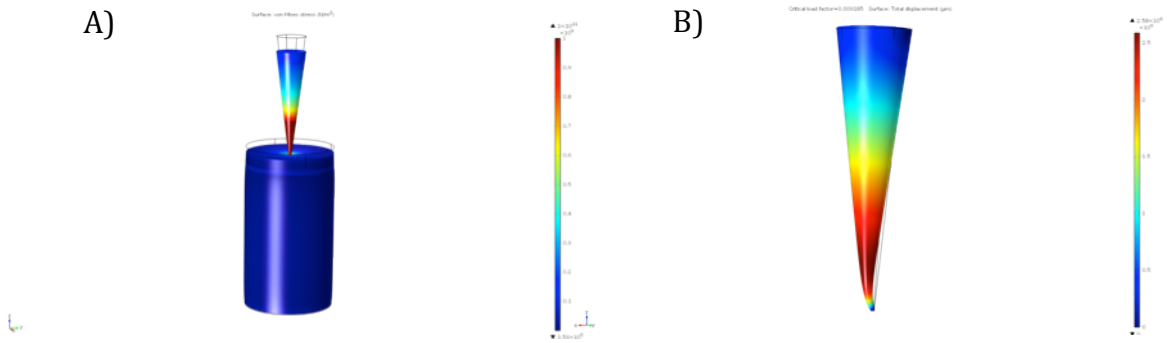

Figure 3: A) Finite element analysis of the surface von Mises stress when axial load, 5 N, is applied on the base of a CMC / MAL microneedle of conical shape. The skin is simulated as a union of cylindrical structures comprising the epidermis and dermis. B) Buckling mode prediction for a CMC / MAL microneedle when axial load is applied at the base of the microneedle and a fixed constraint is forced at the tip of the microneedle.

The predicted stresses were calculated for a single needle and adapted for the 18 x 18 microneedle array by dividing by the total number of the needles in the array (Table 2). A parametric sweep of applied forces was used until the predicted stress values for the microneedle arrays reached the values of the ultimate tensile strength for their corresponding sugar material. The calculated von Mises stresses for the CMC / SUC microneedles exceeded the ultimate stress value for the material constituent, 2.21e7 Pa, when the applied force > 0.1 N. On the other hand, the von Mises stresses for the more rigid CMC / MAL and CMC / TRD sugar composites, did not reach their ultimate tensile stress values until the applied forces exceeded 17 N and 13 N, respectively.

Table 2. Calculated von Mises stresses for a CMC / SUC, CMC / MAL and CMC / TRD microneedle. Values were measured using the Structural Mechanics module of COMSOL Multiphysics for a single microneedle based on which a value was estimated for an 18 x 18 array. The values highlighted in bold indicate the approximate force at which the predicted von Mises stresses reach the ultimate tensile strength of the material.

F (N)	**SUC – von Mises (Pa)**		**MAL-von Mises (Pa)**		**TRD-von Mises (Pa)**	
	Per needle	18x18 array	Per needle	18x18 array	Per needle	18x18 array
0.1	7.40e9	**2.28e7**	1.43e10	4.41e7	1.43e10	4.41e7
1	7.40e10	2.28e8	1.43e11	4.41e8	1.43e11	4.41e8
2	1.48e10	4.57e8	2.86e11	8.83e8	2.86e11	8.83e8
3	2.21e11	6.58e8	4.29e11	1.32e9	4.29e11	1.32e9
4	2.96e11	9.13e8	5.72e11	1.76e9	5.72e11	1.76e9
5	3.70e11	1.14e9	7.17e11	2.21e9	7.15e11	2.21e9
10	7.40e11	2.28e9	1.43e12	4.41e9	1.43e12	4.41e9
13	9.63e11	2.97e9	1.86e12	5.47e9	1.86e12	**5.74e9**
15	1.11e12	3.43e9	2.15e12	6.63e9	1.43e12	4.41e9
17	1.26e12	3.89e9	2.43e12	**7.50e9**	2.43e12	7.50e9

Linear buckling analysis was performed to evaluate the force of failure due to buckling for the three sugar microneedle arrays. The predicted critical load factor, λ, for the microneedle was determined for an applied force of 5 N and the critical buckling force was obtained by multiplying the applied force by the critical load factor. When the applied force is higher than the critical buckling force, or when the critical load factor, λ, has values less than 1, then buckling occurs. The predicted critical load factors for the single microneedles were adapted for an 18 x 18 microneedle array by multiplying by the total number of the needles in the array (Table 3).

Table 3. Calculated critical load factors, λ, and critical loads, $F_{crit.}$, for a CMC / SUC, CMC / MAL and CMC / TRD microneedle. Values were measured using the Structural Mechanics module of COMSOL Multiphysics for a single microneedle based on which a value was estimated for an 18 x 18 array. The applied force used for the buckling analysis was 5N.

Sugar	λ		$F_{crit.}$ **(N)**
	Per needle	18x18 array	18x18 array
CMC/SUC	2.72e-5	0.0088	0.04
CMC/MAL	0.0092	3.0	15
CMC/TRD	0.0070	2.3	11

The critical buckling force for the array is estimated by multiplying the predicted critical load factors by the applied load. Based on these results, the critical buckling force for the sugar microneedle arrays was calculated to be 0.04 N for CMC / SUC, 15 N for CMC / MAL and 11 N for CMC / TRD. This indicates that microneedle arrays made of CMC / SUC are likely to experience failure due to buckling as the required force of insertion to the skin [24] is higher than their critical buckling force. On the other hand, the values of the critical buckling forces for the CMC / MAL and CMC / TRD microneedles are much higher than the insertion forces indicating that both arrays can be inserted in the skin without failing from buckling. Figure 3B shows the predicted buckling mode and the point-of-failure, which is the area coloured in red. The same buckling mode has been predicted for all the sugar microneedles.

3.3 Skin penetration studies

Skin penetration was tested in *ex vivo* porcine skin samples with the aim of assessing both ability and depth of microneedle penetration. Disruption of stratum corneum was evident for all skin samples and the breach locations were observed with separation distances of approximately 550 μm, consistent with the microneedle array spacing (Fig. 4B). Furthermore, microscopic

observation of the microneedles after skin puncture showed that the microneedles remained intact. Evidence of bending at microneedle tips was clear throughout the array for the CMC / SUC arrays while for the CMC / MAL and CMC / TRD arrays tip-bending was observed only for microneedles located at the edge of the arrays (Fig. 4A).

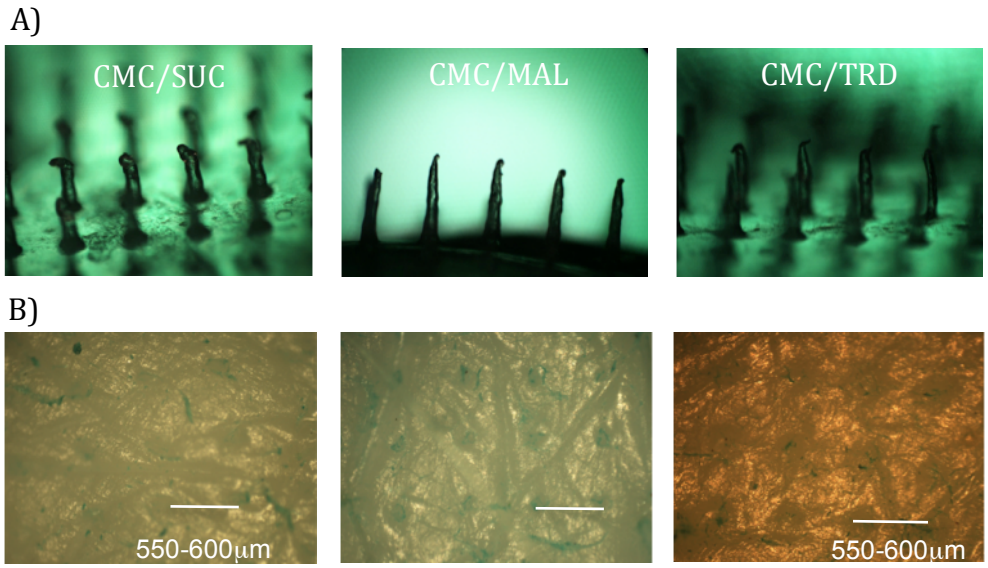

Figure 4: A) Microscopic images of microneedle arrays of CMC / SUC, CMC / MAL, CMC / TRD, after being inserted into the skin for 30 sec B) Microscopic images of the punctured skin after testing with CMC / SUC, CMC / MAL and CMC / TRD microneedles, for 30 sec.

Confocal microscopy was subsequently used to evaluate the depth of skin penetration using fluorescently labelled microneedles. Maximum fluorescence depth at 5 skin breach locations, per sample, was measured and a mean value was determined (Fig. 5). Maximum mean fluorescence depths of 35 μm for CMC / SUC microneedles, 90 μm for CMC / MAL microneedles and 65 μm for the CMC / TRD microneedles were recoded. The actual depth of skin penetration is likely to be deeper than that measured by confocal microscopy since the technique has limited detection sensitivity due to

significant attenuation and scatter of both excitation and emission wavelengths by the epidermis [25].

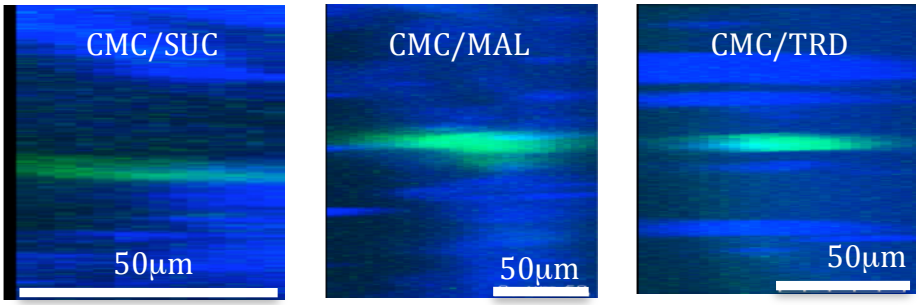

Figure 5: Z-stack images of punctured skin after being tested with fluorescently-labelled microneedles of CMC / SUC, CMC / MAL, and CMC / TRD sugar compositions, for 10min. Green colour represents the recorded fluorescence due to the diffusion of AlexaFluor488 from the microneedles to the skin. The penetration direction is from left to right where the surface of the skin is at the left-hand side.

3.4 Drug delivery studies

Preliminary studies showed that a maximum concentration of 10 % w/w propanolol hydrochloride could be incorporated into the microneedles without compromising their mechanical properties. In subsequent experiments it was incorporated into the microneedle matrix at 5 % w/w. To investigate the release of propanolol from the microneedles, a 30 h permeation experiment was performed and drug permeating into and across full thickness *ex vivo* porcine skin was determined. In this study the use of full thickness skin was deemed more appropriate than dermatomed skin since an aim of the experiment was to understand what effect dissolving-microneedle delivery has on the relationship between local and transdermally delivered drug. There is also evidence in the literature that full-thickness skin is a better model of skin permeation and penetration than dermatomed skin [26]. The drug-loaded

microneedles were compared to controls comprising of flat disks (no microneedles) of the same sugar/propanolol formulation.

Conversely, the permeation of propanolol after application of the CMC / TRD microneedles was slightly slower rate than the control. Total delivery after 30 h was greatest for the CMC / MAL and CMC / SUC microneedles (1.4 % and 1.0 % respectively) (Fig. 6C), however significance was only shown for the CMC / MAL microneedles ($P = 0.044$, microneedle versus control at 30 h). In comparison, the CMC / TRD microneedles delivered 0.3 % of the propanolol dose after 30 h. These values are relative to the applied dose, this includes drug present in the microneedle and in the microneedle-backing layer with drug in the backing layer being a significant proportion of the total. If an assumption is made that the applied dose is that which is present in the dissolving microneedles, then the % delivered increases by a factor of 10. When compared to their respective controls, CMC / MAL microneedles resulted in the largest increase in total propanolol delivery (366 % increase versus 100 % increase and 25 % decrease for CMC / SUC and CMC / TRD, respectively).

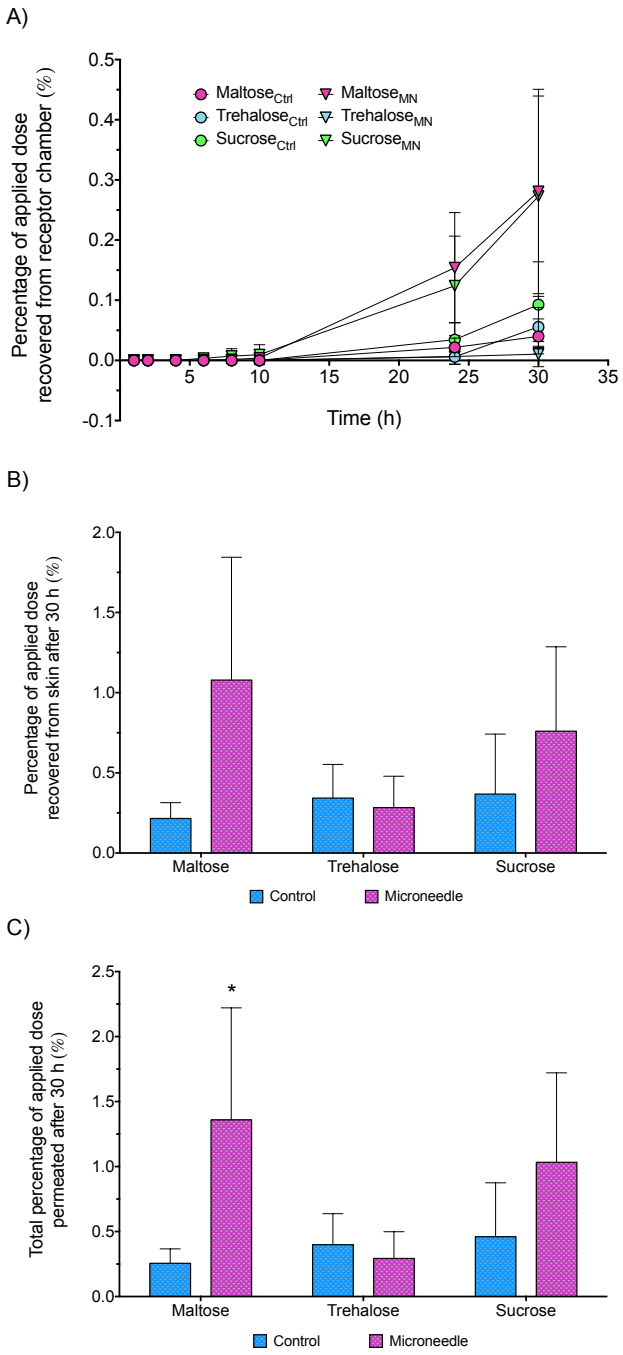

Figure 6: Delivery of propanolol into and across full thickness *ex vivo* porcine skin from microneedle arrays and control sugar disks made of CMC / MAL, CMC / TRD and CMC / SUC. A) Comparative permeation profile of propanolol loaded microneedles and controls over 30 h. (B) Percentage of propanolol dose recovered from the skin after 30 h. C) Total percentage of propanolol dose delivered to the skin after 30 h (calculated as the sum of drug in the skin and receptor chamber of the Franz-type cell, * $P < 0.05$). For all figures, n = 4 ± SD.

4. Discussion

Sugars are particularly attractive materials for preparing dissolvable microneedles for the delivery of biological agents since sugars are known to improve biomolecule stability. While sugar-based microneedles are readily loaded with biomacromolecules, the resultant device can have stability problems due to its inherent hygroscopic nature, which results in poor storage prognosis at ambient relative humidities. One way of increasing the long-term stability of sugar microneedles is by combining different substituents of varying elasticity and rigidity. In this study carboxymethylcellulose was co-formulated with sugars to bring about improved storage profiles, in addition the inclusion of cellulose gave rise to stiffer materials [27] resulting in mechanically stronger microneedles [12].

Most published studies on sugar microneedles focus on the delivery potential of devices and not on structural aspects of the microneedles themselves. Systematic mechanical analysis of dissolving microneedles is desirable since it would provide an insight into their practical usefulness and levels of effectiveness in a specific application. In this study we sought to manipulate the elastic properties of a range of different sugar microneedles by co-formulating with carboxymethylcellulose. The mechanical properties of the resulting microneedles were evaluated and correlated against their effectiveness to penetrate skin and the delivery of propanolol ‘to’ and ‘through' full thickness porcine skin.

When microneedles are applied to the surface of the skin they can easily be deformed due to the viscoelastic nature of the skin. As such, the design and choice of material has a critical role in determining whether the

microneedles will effectively penetrate when applied to the skin. Assuming that a microneedle is loaded into the skin with coaxial force, then the typical forces that the microneedle will experience are compressive and buckling. In real applications however, lateral movements are also generated giving rise to bending forces. In an ideal situation the bending forces can be ignored so that the compressive and buckling become the main forces acting on the microneedles. For slender, high aspect ratio microneedle geometries, buckling is most likely to be the major mode of mechanical failure [16]. Accordingly in this study, buckling was observed and was more prominent for the sugar microneedles made of CMC / SUC whereas, none of the microneedles tested experienced failure from fracture.

The critical buckling load for a microneedle, *F*, can be described by Euler's buckling formula for a cylindrical column, (Eq. 1), where *E*, is the elasticity factor of a material described by Young's modulus, *d*, the area moment of inertia that is dependent on geometry, *K*, the column effective factor that is determined by the boundary conditions and *L* the unsupported length of the column.

$$F = \frac{E\pi^3 d^4}{64(KL)^2} \qquad Eq.1$$

All other factors being equal, as it is in this case since all sugar microneedles possess the same geometry, then based on Euler's formula the elasticity of the material will determine the critical buckling load. Consequently, based on the Young's modulus values for the three sugar constituents (Table 1), the critical load that CMC / SUC microneedles can withstand before buckling would be much lower than that for CMC / TRD and CMC / MAL microneedles.

Based on the simulations the CMC / SUC microneedles are likely to buckle when the applied axial force exceeds 0.04 N. The typical force that is required for a microneedle array to puncture the skin is around 0.1 N [24], depending on microneedle material and geometry, consequently the CMC / SUC microneedles should fail from buckling before skin penetration is achieved. Interestingly, the predicted buckling mode for the microneedles shows the point of failure to be slightly above the tip (Fig. 3B). This indicates that even in the event when the insertion force is higher than the critical buckling threshold, as is the case of the CMC / SUC microneedles, the microneedles may still puncture the skin and penetrate to a certain depth before failing. The depth of skin penetration can be correlated to the critical buckling force. Best skin penetration was demonstrated by CMC / MAL microneedles. These also had the highest predicted critical buckling force (closely followed by the CMC / TRD microneedles). Finally, the CMC / SUC microneedles, that penetrated least effectively, had the lowest predicted critical buckling force.

Although mechanical studies suggested that the CMC / SUC microneedles would be least effective in penetrating the skin, drug delivery studies showed that these microneedles performed similarly to the CMC / MAL formulation in terms of the proportion of the applied dose of propanolol that they delivered. Furthermore, in contrast to that predicted by the mechanical studies, the CMC / TRD microneedles delivered the least amount of propanolol, having no statistical difference versus the control. One of the reasons for these differences may be the dissolution rate of the sugar microneedles within the skin. One could argue that the CMC / SUC microneedles dissolve at a faster rate in the skin and thus delivering a greater

amount of drug at a given time. Another factor that should be considered is the diffusion of propanolol through the skin the rate of which may depend on the microneedle formulation. For example, when comparing the CMC / sugar controls, a larger percentage of applied dose permeated was recorded for the CMC / SUC control compared to the CMC / MAL and CMC / TRD controls, (Fig. 6A). One of the major differences between trehalose and maltose and sucrose is that trehalose forms larger hydration spheres and this has been correlated to the extra stability that trehalose offers to biomolecules [28,29]. It is suggested that sugars form multiple hydrogen bonds with the polar groups of the biomolecules by replacing water from their hydration sphere and consequently, leading to biomolecule stabilisation [30]. It is thus reasonable that the microneedle sugars establish higher-order hydrogen-bonded complexes with propanolol that may affect its diffusion rate from the microneedles to and through the skin. Given the larger hydration sphere of TRD this effect may be more pronounced for the CMC / TRD formulation thus providing another possible explanation for the unexpectedly poor performance of this microneedle.

Conclusions

In this study we undertook experimental and computational analyses to investigate the mechanical properties of sugar microneedles and additionally performed a comparative study of their ability to deliver drug to the skin. Both predictions and experiments showed that microneedles made of CMC / MAL are superior to those made of CMC / SUC and CMC / TRD in terms of the mechanical strength and drug delivery properties. Simulation analyses revealed the main reason for mechanical failure to be buckling and

showed a correlation between the Young's modulus of the sugar constituents and the predicted critical buckling load of the microneedles and the depth of skin penetration. The drug delivery experiments showed that other factors in addition to mechanical strength such as, diffusivity and interactions between drug and microneedle component are also significant, highlighting the importance of considering both the physical and chemical properties of materials in microneedle design.

Acknowledgments

The assistance of Dr Emmanuel Brousseau with SEM and Dr Edward Sayers with confocal microscopy is gratefully acknowledged. This study was supported by the Marie Curie Industry-Academia Partnerships and Pathways FP7-PEOPLE-2009-IAPP-251630 grant, *HIPODERM*.

References

[1] Y.-C. Kim, J.-H. Park, M.R. Prausnitz, Microneedles for drug and vaccine delivery, Adv. Drug Deliv. Rev. 64 (2012) 1547–1568.

[2] M. Pearton, V. Saller, S.A. Coulman, C. Gateley, A.V. Anstey, V. Zarnitsyn, et al., Microneedle delivery of plasmid DNA to living human skin: Formulation coating, skin insertion and gene expression, J. Controlled Release. 160 (2012) 561–569.

[3] E.E. Peters, M. Ameri, X. Wang, Y.-F. Maa, P.E. Daddona, Erythropoietin-coated zp-microneedle transdermal system: Preclinical formulation, stability, and delivery, Pharm Res. 29 (2012) 1618–1626.

[4] Y.C. Kim, F.-S. Quan, R.W. Compans, S.-M. Kang, M.R. Prausnitz, Formulation of microneedles coated with influenza virus-like particle vaccine, AAPS PharmSciTech. 11 (2010) 1193–1201.

[5] C. Edens, M.L. Collins, J. Ayers, P.A. Rota, M.R. Prausnitz, Measles vaccination using a microneedle patch, Vaccine. 31 (2013) 3403–3409.

[6] W.C. Weldon, M.P. Martin, V.G. Zarnitsyn, B.Z. Wang, D.G. Koutsonanos, I. Skountzou, et al., Microneedle vaccination with stabilized recombinant influenza virus hemagglutinin induces improved protective immunity, Clin Vaccine Immunol. 18 (2011) 647–654.

[7] A. Vrdoljak, M.C. McGrath, J.B. Carey, S.J. Draper, A.V.S. Hill, C. O'Mahony, et al., Coated microneedle arrays for transcutaneous delivery of live virus vaccines, J. Controlled Release. 159 (2012) 34–42.

[8] F.E. Pearson, C.L. McNeilly, M.L. Crichton, C.A. Primiero, S.R. Yukiko, G.J. Fernando, et al., Dry-Coated Live Viral Vector Vaccines Delivered by Nanopatch Microprojections Retain Long-Term Thermostability and Induce Transgene-Specific T Cell Responses in Mice, PLoS One. 8 (2013) e67888.
[9] S. Kommareddy, B.C. Baudner, S.-J. Oh, S.-Y. Kwon, M. Singh, D.T. O'Hagan, Dissolvable microneedle patches for the delivery of cell-cultured-derived influenza vaccine antigens, J. Pharm. Sci. 101 (n.d.) 1021–1027.
[10] Y.-C. Kim, F.-S. Quan, R.W. Compans, S.-M. Kang, M.R. Prausnitz, Formulation and coating of microneedles with inactivated influenza virus to improve vaccine stability and immunogenicity, J. Controlled Release. 142 (2010) 187–195.
[11] Y.C. Kim, F.-S. Quan, J.M. Song, A. Vunnava, D.G. Yoo, K.M. Park, et al., Influenza immunization with trehalose-stabilized virus-like particle vaccine using microneedles, Proc Vaccinol. 2 (2010) 17–21.
[12] V. Bachy, C. Hervouet, P.D. Becker, L. Chorro, L.M. Carlin, S. Herath, et al., Langerin negative dendritic cells promote potent CD8+ T-cell priming by skin delivery of live adenovirus vaccine microneedle arrays, PNAS. 118 (2013) 8–13.
[13] J.W. Lee, S.O. Choi, E.I. Felner, M.R. Prausnitz, Dissolving microneedle patch for transdermal delivery of human growth hormone, Small. 7 (2011) 531–539.
[14] R. Aggarwal, C.R. Johnston, Geometrical effects in mechanical characterizing of microneedle for biomedical applications, Sens. Actuators B. 102 (2004) 226–234.
[15] J.W. Lee, J.-H. Park, M.R. Prausnitz, Dissolving microneedles for transdermal drug delivery, Biomaterials. (2008) 2113–2124.
[16] J.-H. Park, M.R. Prausnitz, Analysis of the Mechanical Failure of Polymer Microneedles by Axial Force, J. Korean Phys. Soc. 56 (2010) 1223–1227.
[17] R.F. Donnelly, M.J. Garland, D.I.J. Morrow, K. Migalska, T.R.R. Singh, R. Majithiya, et al., Optical coherence tomography is a valuable tool in the study of the effects of microneedle geometry on skin penetration characteristics and in-skin dissolution, J. Controlled Release. 147 (2010) 333–341. doi:10.1016/j.jconrel.2010.08.008.
[18] C.J. Martin, C.J. Allender, K.R. Brain, A. Morrissey, J.C. Birchall, Low temperature fabrication of biodegradable sugar glass microneedles for transdermal drug delivery applications, J. Controlled Release. 158 (2012) 93–101.
[19] M. Geerligs, L. van Breemen, G. Peters, P. Ackermans, F. Baaijens, C. Oomens, In vitro indentation to determine the mechanical properties of epidermis, J. Biomech. 44 (2011) 1176–1181.
[20] Y. Hara, Y. Masuda, T. Hirao, N. Yoshikawa, The relationship between the Young's modulus of the stratum corneum and age: a pilot study, Skin Res. Technol. Off. J. Int. Soc. Bioeng. Skin ISBS Int. Soc. Digit. Imaging Skin ISDIS Int. Soc. Skin Imaging ISSI. 19 (2013) 339–345. doi:10.1111/srt.12054.

[21] T. Miyano, Y. Tobinaga, T. Kanno, Y. Matsuzaki, H. Takeda, M. Wakui, et al., Sugar micro needles as transdermic drug delivery system, Biomed. Microdevices. 7 (2005) 185–188.
[22] K. Lee, C.Y. Lee, H. Jung, Dissolving microneedles for transdermal drug administration prepared by stepwise controlled drawing of maltose, Biomaterials. 32 (n.d.) 3134–3139.
[23] R.B. Groves, S.A. Coulman, J.C. Birchall, S.L. Evans, Quantifying the mechanical properties of human skin to optimise future microneedle device design, Comput. Methods Biomech. Biomed. Engin. 15 (2012) 73–82.
[24] S.P. Davis, B.J. Landis, Z.H. Adams, M.G. Allen, M.R. Prausnitz, Inserion of microneedles into skin: measurement and prediction of insertion force and needle fracture force, J. Biomech. 37 (2004) 1155–1163.
[25] L.J. Mortensen, C.E. Glazowski, J.M. Zavislan, L.A. DeLouise, Near-IR fluorescence and reflectance confocal microscopy for imaging of quantum dots in mammalian skin, Biomed. Opt. Express. 2 (2011) 1610–1625. doi:10.1364/BOE.2.001610.
[26] C.M. Heard, C. Screen, Probing the permeation enhancement of mefenamic acid by ethanol across full-thickness skin, heat-separated epidermal membrane and heat-separated dermal membrane, Int. J. Pharm. 349 (2008) 323–325. doi:10.1016/j.ijpharm.2007.08.006.
[27] F. Bassam, P. York, R.C. Rowe, R.J. Roberts, Young's modulus of powders used as pharmaceutical excipients, Int. J. Pharm. 64 (1990) 55–60.
[28] N. Ekdawi-Sever, J.J. de Pablo, E. Feick, E. von Meerwall, Diffusion of Sucrose and a,a-Trehalose in Aqueous Solutions, J Phys Chem A. 107 (2003) 936–943.
[29] A. Lerbret, P. Bordat, F. Affouard, M. Descamps, F. Migliardo, How homogeneous are the trehalose, maltose and sucrose water solutions? An insight from Molecular Dynamics simulations, J Phys Chem B. 109 (2005) 11046–11057.
[30] J.F. Carpenter, J.H. Crowe, An infrared spectroscopic study of the interactions of carbohydrates with dried proteins, Biochemistry (Mosc.). 28 (1989) 3916–3922.